# Synthesis of Highly Crystalline $sp^2$-Bonded Boron Nitride Aerogels

**Michael Rousseas,[†,‡] Anna P. Goldstein,[†,‡,§] William Mickelson,[†,⊥] Marcus A. Worsley,[∥] Leta Woo,[∥] and Alex Zettl[†,‡,⊥,*]**

[†]Department of Physics, University of California, Berkeley, California 94720, United States, [‡]Materials Science Division, Lawrence Berkeley National Laboratory, Berkeley, California 94720, United States, [§]Department of Chemistry, University of California, Berkeley, California 94720, United States, [⊥]Center of Integrated Nanomechanical Systems, Berkeley, California 94720, United States, and [∥]Physical Sciences Directorate, Lawrence Livermore National Laboratory, Livermore, California 94550, United States

**ABSTRACT** $sp^2$-Bonded boron nitride aerogels are synthesized from graphene aerogels *via* carbothermal reduction of boron oxide and simultaneous nitridation. The color and chemical composition of the original gel change dramatically, while structural features down to the nanometer scale are maintained, suggesting a direct conversion of the carbon lattice to boron nitride. Scanning and transmission electron microscopies reveal a foliated architecture of wrinkled sheets, a unique morphology among low-density, porous BN materials. The converted gels display a high degree of chemical purity (>95%) and crystalline order and exhibit unique cross-linking structures.

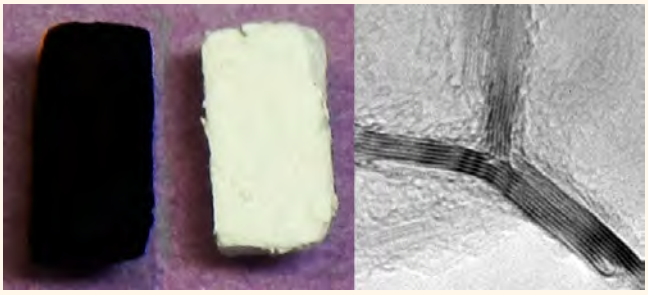

**KEYWORDS:** boron nitride · porous · aerogels · $sp^2$-bonded · carbothermal reduction

Porous, high surface area nanostructured carbon-based materials play vitally important roles in research and industry,[1,2] in products as wide ranging as filtration systems,[3] poison control,[4] and supercapacitors, and other alternative energy technologies.[5−7] Boron nitride (BN) forms bonding configurations similar to carbon and may serve as an alternative in certain applications. While sharing many of the same robust mechanical and thermal properties of graphite,[8,9] the polar nature of the boron−nitrogen bond in $sp^2$-bonded BN makes it an wide band gap insulator,[10] with different chemistry on its surface. For example, BN-based materials are significantly more resistant to oxidation than graphene-based materials.[11] BN also has enhanced physisorption properties due to the dipolar fields near its surface.[12] High specific surface area (SSA) BN has been shown to surpass carbon in its ability to store gases such as hydrogen[13−18] and is a very effective and reusable cleanup agent for hydrocarbons.[19] Like the silica which forms the backbone of more common aerogels, BN is optically transparent,[20] and porous BN structures have recently been shown to have small and adjustable dielectric constants,[21] a useful feature in traditional aerogel applications. Also, despite their relative chemical inertness, BN surfaces can be functionalized,[22,23] allowing for their incorporation into composites,[24] as well as their use as scaffolds for nanoparticles in catalysis and other applications.[25]

Previous synthetic routes for BN aerogels and related mesoscale assemblies have included gelation of colloidal BN suspensions,[26] templated growth from existing porous structures such as zeolites[27] and metal foams,[21] and various high-temperature reactions of boron- and nitrogen-containing compounds.[13,14,16,17,28−30] Despite a number of promising fields of application, research in this area has been slow due to the often toxic and volatile precursors involved and the limited synthetic routes to high-quality BN. Furthermore, these synthesis methods have generally resulted in compounds of random BN phases and disordered or turbostratic stacking of atomic layers. Recent advances in crystalline carbon nanotube and graphene-based aerogels have shown significant improvement in the materials performance over amorphous

* Address correspondence to azettl@berkeley.edu.

Received for review May 14, 2013 and accepted September 8, 2013.

**Published online September 09, 2013**
**10.1021/nn402452p**

carbon structures,[31−33] suggesting that BN-based materials may also benefit from increased structural order.

We report here on the synthesis and characterization of high specific surface area (SSA), low-density aerogels comprosed locally of few atomic-layer sheets of $sp^2$-bonded BN. The aerogels were derived from graphene aerogel precursors and show a high degree of crystalline order and chemical purity. Our process uses only common, nonhazardous reactants; moreover, it elucidates a remarkable process in which carbon nanostructures can be completely converted to BN while maintaining their macro- and nanoscale morphologies.

Graphene aerogels, with typical mass densities of 60−150 mg/cm$^3$ and SSA of around 1200 m$^2$/g, are first prepared using a previously published method.[33] They are then placed together with boron oxide in a graphite crucible and heated rapidly in an induction furnace under nitrogen flow. At sufficiently high temperatures, the graphene sheets of the starting aerogel react with boron oxide and nitrogen to form $sp^2$-bonded BN, nominally according to the equation

$$B_2O_3 + 3C + N_2 \rightarrow 2BN + 3CO \quad (1)$$

This reaction, one of the earliest known synthetic routes to pure BN,[34] is widely used in industry[35,36] and has been previously used in the conversion of other forms of nanostructured carbon.[37,38] At temperatures above 1500 °C, the boron oxide is believed to react purely in the vapor phase and BN is found to be the only solid product.[39] Our operating temperature is in the range of 1600−1800 °C in order to provide sufficient vapor pressure of boron oxide to allow the reaction to occur at a reasonable rate and to ensure a highly pure BN aerogel. Moreover, our attempts at conversion at lower temperatures tend to result in gels with very low surface area. In addition, we take extra care to avoid contact between the aerogel and liquid boron oxide, so as to prevent any potential damage to the pore structure from capillary forces.

## RESULTS AND DISCUSSION

Figure 1 shows a photograph of a precursor graphene aerogel alongside a converted BN aerogel. The converted sample has maintained its original size and macroscopic shape. There is, however, a dramatic change in color from black to white, which is uniform throughout the cross section of the sample. The BN aerogel is somewhat more fragile and brittle than its graphene-based precursor. While eq 1 would imply an increase in the mass upon conversion, we observe instead a small degree of mass loss, of around 10%, which is consistent with other studies of conversion of graphitic materials to boron nitride.[39] This may be due to the formation of cyanogen, which begins to proceed rapidly at these temperatures, especially for high surface area materials.[40]

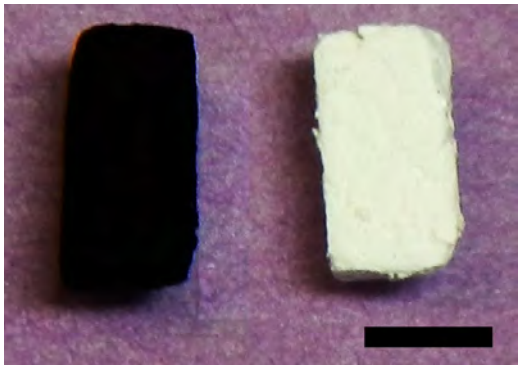

**Figure 1. Photograph of a precursor graphene aerogel (left) and a converted BN aerogel (right). The color of the aerogel undergoes a significant color change, from pitch black to bright white, indicating a major change in the chemical composition. However, the overall macroscopic geometry of the samples remains unchanged. Samples shown have roughly square cross sections. Scale bar is 5 mm.**

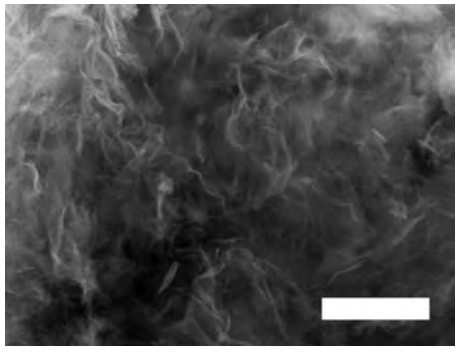

**Figure 2. SEM image of a BN aerogel. The structure is composed of many ultrathin, wrinkled sheets several micrometers long and folded into each other, forming slit-shaped macropores. Scale bar is 5 $\mu$m.**

Figure 2 is a scanning electron microscope image showing the mesoscale structure of the BN aerogel assembly. The foliated architecture is very similar to that of the starting graphene aerogel.[32,33] Thin sheets several tens of micrometers on a side are found crumpled together, forming slit-shaped macropore structures. As in the case of graphene aerogels, these structures are stable despite being only a few atomic layers thick owing to the relatively high stiffness of few-layer BN sheets.[41,42]

Figure 3 shows a series of transmission electron microscopy (TEM) images of the starting graphene aerogels (a and c) and the converted boron nitride samples (b and d). Additional images can be found in Figures S1 and S2 of the Supporting Information. In some regions, two or more sheets are found lying atop one another, as in the left part of Figure 3a. We find that the morphology on the 100 nm scale has not been significantly altered upon conversion to BN. In both cases, the material is composed of wrinkled sheets with facets on the order of hundreds of square nanometers and several atomic layers thick.

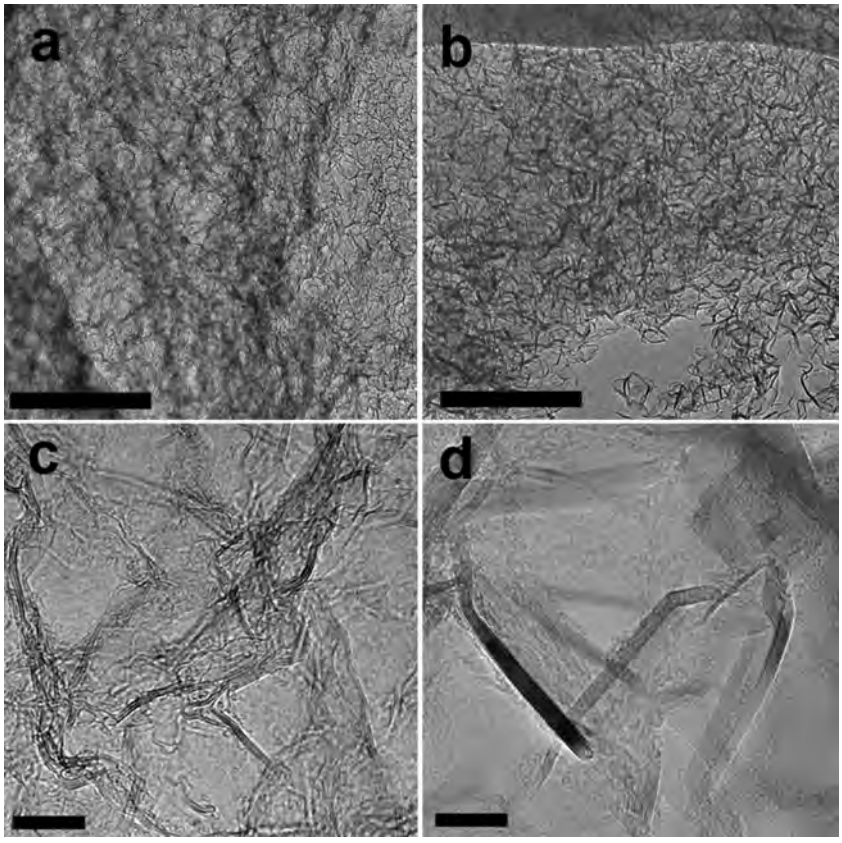


**Figure 3. TEM images of original graphene aerogel (a,c) and converted BN aerogel (b,d). The lower-magnification TEM images (a,b) show that both aerogels are porous with feature sizes of about 30 nm. The higher-magnification TEM images (c,d) show that the aerogels comprise layered structures, indicated by the parallel, dark fringes. Upon conversion to BN, the layered structures become more crystalline with sharp transitions between the facets (d), compared to the more meandering layers observed in the graphene aerogels (c). In addition, the average number of wall for the constituent sheets increases from 2 to 3 in the case of the graphene gels to 6−8 for the BN gels. Scale bars are 200 nm (a,c) and 10 nm (c,d).**

Figure 3c shows a high-magnification image of the larger area shown in 3a. The lattice fringes seen throughout the sample are due to portions of the graphene aerogel's sheets oriented perpendicular to the electron beam or to sections of the sheets that have folded onto themselves, as has been previously observed in single-layer graphene.[43,44] These features reveal that the sheets of the graphene aerogel are made up of two to three atomic layers on average. Interlayer spacing is found to vary widely, ranging from 0.37 to 0.43 nm; it is consistently found to be larger than 0.335 nm, which is that of highly crystalline hexagonal graphite.

Analogous features in the converted BN aerogel appear straighter and more ordered than those of the graphene aerogel. In Figure 3d, we see atomically straight edges 40 nm and longer, whereas such features are at most 10 nm in the graphene aerogel precursor. Interestingly, in addition to improving the crystalline order, the conversion process appears to increase the thickness of the sheets, which now number six to eight atomic layers on average. In the case of the BN aerogel, the interlayer spacing is found to be to be 0.331 ± 0.003 nm and is highly consistent throughout the sample. This interlayer spacing is confirmed by the gels' X-ray diffraction (XRD) spectrum, shown in Figure S3, and is consistent with both hexagonal and rhombohedral boron nitride. Moreover, the appearance of rounded edge terminations at the ends of these linear features indicates that at least some of these structures are extended, vertical facets standing perpendicular to the average plane of the sheet.

Figure 4 shows a high-magnification TEM image of a cross-link in a converted BN aerogel. The sheets here form a "Y" junction, wherein neighboring sheets share one or more atomic layers. Some layers extend fully from one sheet to the next, while others overlap by several nanometers. Such junctions tend to be found in regions of the sample where two sheets lay atop one another. Additional examples of these junctions of varying geometries are shown in Figure S4. The aerogel thus appears to be an interlaminated structure, where shared, $sp^2$-bonded layers of BN form the cross-links between the sheets.

The elemental composition and in-plane bonding structure of the BN aerogel are analyzed *via* electron energy loss spectroscopy (EELS). The resulting spectrum, shown in Figure 5a, shows a distinct nitrogen K

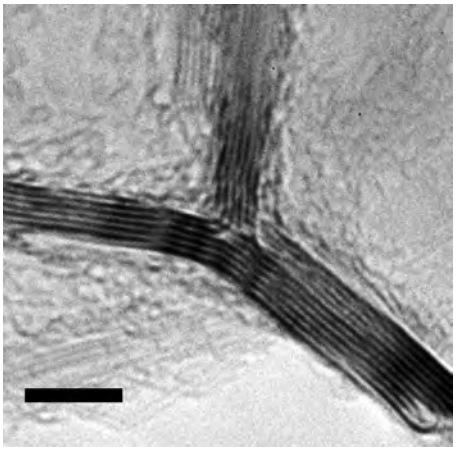

Figure 4. High-resolution TEM image of a cross-link in a BN aerogel. The atomic layers of BN extend uninterrupted from all three aerogel sheets, showing that these extended structures are held together by covalent $sp^2$ bonds. Similar structures of varying geometries are found throughout the BN aerogel samples. Scale bar is 5 nm.

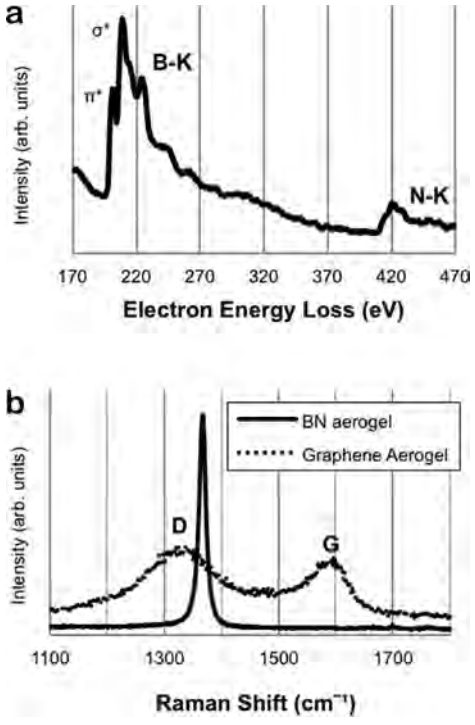


Figure 5. (a) Electron energy loss spectrum taken from a converted BN aerogel. The strong peak near 200 eV is attributed to boron, with edge features consistent with $sp^2$-bonded BN; the peak near 400 eV is attributed to nitrogen. Noticeably absent is any distinguishable feature near 290 eV which would indicate the presence of carbon. The calculated ratio of boron to nitrogen is nearly 1:1, and the carbon concentration is below the resolution of the spectrometer (<5%). (b) Raman spectrum of the BN aerogel (solid line) and the graphene-based precursor (dotted line). The graphene aerogel spectrum shows broad peaks for the D and G bands in graphene, as observed in previous reports of graphene aerogel synthesis. The BN spectrum shows a single sharp peak at 1366 $cm^{-1}$, indicating that the BN aerogels have highly crystalline $sp^2$ bonding.

edge at 401 eV and boron peaks arising from $\pi^*$ and $\sigma^*$ states at around 188 eV, which are indicative of well-ordered, $sp^2$-bonded BN.[45,46] Importantly, the absence of any carbon K edge at 284 eV confirms that the original graphene aerogel has been completely consumed in the conversion process. The boron to nitrogen atomic ratio for this sample is $0.97 \pm 0.14$, while the carbon content is less than 5%.

The dramatic change in the chemical composition and crystalline order upon converting graphene aerogel to BN aerogel is also evident in the Raman spectra of the respective materials, shown in Figure 5b. The graphene-based material shows strong D (1329 $cm^{-1}$) and G (1582 $cm^{-1}$) peaks with weak, broad D′ and G′ features, as observed previously for other graphene aerogels synthesized by a similar method.[32] After conversion to BN, these peaks are entirely absent and replaced by a single peak at 1366 $cm^{-1}$, as is also observed in reference samples of pyrolytic hexagonal BN.[41] There is no noticeable shift in the peak, as is expected for BN sheets more than four layers thick.[20] This $E_{2g}$ peak is due to the same in-plane phonons that give rise to the G peak in graphene. The fwhm of 14 $cm^{-1}$ is indicative of highly crystalline $sp^2$-bonded BN. The small increase in peak width from 9.1 $cm^{-1}$ is likely related to shortened phonon lifetimes due to the nanoscale wrinkles in the sheets of the aerogel.[47]

The increase in crystalline order, as well as the increase in the wall thickness compared to the graphene precursor, is also seen in the conversion of other nanostructured carbon materials[37,38] and appears to be a consequence of the specifics of the conversion reaction. The increase in the number of layers making up the BN aerogel, coupled with the small decrease in density, is corroborated by a reduction of the SSA. For one particular sample, the mesopore surface area (2−50 nm pore width) derived from nitrogen adsorption isotherms, shown in Figure S5, and calculated using the Brunauer−Emmett−Teller (BET) model,[48] is reduced from 1158 $m^2/g$ for the graphene precursor to 431 $m^2/g$ for the BN aerogel.

The increase in sheet thickness, along with the preservation of the macro- and mesoscale features of the gel, suggests a mechanism for the conversion process. We propose that the graphene aerogel serves as a sacrificial template, such that the boron oxide is reduced and immediately nitridated on its surface, forming a sheet-like BN structure that mimics the original graphene architecture. Evidence of surface formation of BN has been seen in other studies, where similar preservation of surface morphologies is observed,[49] and where nanocrystallites are seen to decorate the surface of activated carbon and graphite when the amount of boron oxide is limited.[50] In our case, boron oxide vapor can be reduced on both sides of the two- or three-layer thick graphene sheets. Returning to eq 1, we conclude that the process of

carbothermal reduction followed by nitridation results in an increase of sheet thickness of approximately four-thirds since three unit cells of the graphene lattice are replaced by four of the $sp^2$-bonded BN. Subsequently, these sheets either fold on themselves, doubling their thickness and creating the vertical facets six to eight layers thick seen in our TEM images, or pair with their neighbors, forming the cross-linking structures discussed above. Alternately, it is possible that these folds and cross-links are already present in the graphene aerogel and coalesce and are reinforced by the conversion process.

Finally, it should be noted that formation of BN *via* carbothermal reduction of boron oxide is typically surface-passivated,[37] and thus conventionally additional promoters such as various metal oxides are necessary to obtain appreciable conversion yield.[51,52] Here this is not the case. The exceptionally high SSA of our starting graphene aerogels lends itself particularly well to the conversion process, and as such, no additional promoters are here necessary to take the reaction to completion. Nor is it necessary to purify the product by, for example, burning off residual carbon in air;[53] to our knowledge, this work is the first demonstration of the complete conversion of a macroscopic, monolithic graphitic structure to boron nitride.

## CONCLUSIONS

The successful, complete conversion of porous crystalline graphene material to similarly structured BN by means of an inexpensive and nontoxic process opens numerous possibilities in the research and development of new nanostructured BN materials. The growing number of applications for porous BN demands new methods for synthesis. The work presented here demonstrates that the mesoscale architecture as well as the nanoscale morphology of porous materials can be well maintained through conversion to BN and can lead to unique interlinking structures. This work also helps elucidate some of the details of the carbothermal reduction process. Further control of carbon–BN conversion can lead to advances in fabrication of nanoscale electronics, where BN has been shown to be an ideal substrate for graphene-based devices,[54] and to development of BN/graphene heterostructures, a topic of intense current research.[55] Purely two-dimensional circuits using BN as a dielectric barrier are also being actively explored.[56]

## METHODS

**Synthesis of Graphene Aerogels.** Graphene oxide powder (Cheap Tubes Inc., 0.2 g) is mixed with deionized water (16.7 mL) in a 20 mL glass vial and sonicated to reach a smooth liquid consistency. Ammonium hydroxide (3.3 mL, 28 wt % solution) is added and mixed well. The vial is sealed and heated at 85 °C for 40 h, resulting in a monolithic hydrogel. The gel is then soaked sequentially in deionized water and high-purity isopropyl alcohol. Solvent is removed by supercritical $CO_2$ drying. The aerogels are then graphitized *via* firing for 3 h at 1100 °C under argon flow.

**Conversion of Graphene Aerogels.** The conversion occurs in a 5 cm diameter by 10 cm tall cylindrical graphite crucible, shown schematically in Figure S6. The aerogels are supported in the middle of the crucible by a graphite cup with holes drilled in the bottom to allow for proper flow of the reactant gases. About 10 g of boron oxide powder (Alfa Aesar A11707) is placed at the bottom of the crucible, which is then heated under nitrogen flow (1500 sccm) in a radio frequency induction furnace to between 1600 and 1800 °C. We find that it is important to premelt the powder to eliminate adsorbed water and prevent overbubbling and damaging the sample. Nitrogen is introduced through a central tube which in turn mixes well with the boron oxide vapor and helps to carry it upward toward the aerogels. The conversion is run long enough to allow for all of the boron oxide to evaporate; under these conditions, the evaporation rate of boron oxide is between 200 and 500 mg/min.

**Determination of Interlayer Spacing.** Starting from a high-resolution TEM image, the grayscale values of the pixels along a line transecting the given fringes are plotted. For two to three fringes, the resulting curve is fitted to a set of Gaussians using a Levenberg–Marquardt algorithm. For four or more fringes, a discrete Fourier transform is taken using a fast Fourier transform (FFT) alogrithm. The resulting spectrum displays a distinct Fourier peak superimposed on a 1/*f* background. The quoted values and precision for interplanar spacing correspond to the center and width of the peak, respectively.

**Characterization.** TEM images are collected on a JEOL JEM 2010 microscope operating at 80 kV. Samples are prepared by suspending the materials in isopropyl alcohol *via* ultrasonication and then drop-casting onto holey carbon grids; alternately, the grids are simply rubbed gently against a cleaved surface of the gel. EELS is performed using a Phillips CM 200 TEM operating at 200 kV and equipped with a Gatan imaging filter. Raman spectra are collected on a Renishaw inVia spectrometer using a 633 nm excitation laser. Nitrogen adsorption isotherms are measured using a Micromeritics ASAP 2010 porosimeter. XRD is performed using a Bruker D8 Advance X-ray diffractometer using Cu Kα radiation.

*Conflict of Interest:* The authors declare no competing financial interest.

*Acknowledgment.* This work was supported in part by the Director, Office of Energy Research, Office of Basic Energy Sciences, Materials Sciences and Engineering Division, of the U.S. Department of Energy under Contract No. DE-AC02-05CH11231, which provided for structural analysis of the aerogels; by the UC Lab Fees Research Program under Award 12-LR-235323, which provided for detailed TEM analysis; by Lawrence Livermore National Laboratory under the auspices of the U.S. Department of Energy under Contract DE-AC52-07NA27344, which provided for graphene aerogel precursor material; and by the Air Force Office of Scientific Research under Grant X10-8049-C, which provided for the BN conversion process. M.R. thanks D. Golberg and C. Zhi for useful discussions regarding induction furnace operation. W.M. and A.Z. received support from the Center of Integrated Nanomechanical Systems under NSF Grant EEC-0832819. The authors thank T. Pham for assistance in sample preparation, and P. Yang for use of the X-ray diffractometer.

*Supporting Information Available:* Additional characterization, spectra, and electron microscopy images. This material is available free of charge *via* the Internet at http://pubs.acs.org.

## REFERENCES AND NOTES

1. Moreno-Castilla, C.; Maldonado-Hódar, F. J. Carbon Aerogels for Catalysis Applications: An Overview. *Carbon* **2005**, *43*, 455–465.

2. Lee, J.; Kim, J.; Hyeon, T. Recent Progress in the Synthesis of Porous Carbon Materials. *Adv. Mater.* **2006**, *18*, 2073–2094.
3. Yin, C.-Y.; Aroua, M.; Daud, W. Review of Modifications of Activated Carbon for Enhancing Contaminant Uptakes from Aqueous Solutions. *Sep. Purif. Technol.* **2007**, *52*, 403–415.
4. Chyka, P. A.; Seger, D. Position Statement: Single-Dose Activated Charcoal. American Academy of Clinical Toxicology; European Association of Poisons Centres and Clinical Toxicologists. *J. Toxicol. Clin. Toxicol.* **1997**, *35*, 721–741.
5. Frackowiak, E.; Béguin, F. Carbon Materials for the Electrochemical Storage of Energy in Capacitors. *Carbon* **2001**, *39*, 937–950.
6. Qu, D.; Shi, H. Studies of Activated Carbons Used in Double-Layer Capacitors. *J. Power Sources* **1998**, *74*, 99–107.
7. Biener, J.; Stadermann, M.; Suss, M.; Worsley, M. A.; Biener, M. M.; Rose, K. A.; Baumann, T. F. Advanced Carbon Aerogels for Energy Applications. *Energy Environ. Sci.* **2011**, *4*, 656–667.
8. Cohen, M. L.; Zettl, A. The Physics of Boron Nitride Nanotubes. *Phys. Today* **2010**, *63*, 34–38.
9. Dresselhaus, M. S.; Dresselhaus, G.; Charlier, J. C.; Hernández, E. Electronic, Thermal and Mechanical Properties of Carbon Nanotubes. *Philos. Trans. R. Soc., A* **2004**, *362*, 2065–2098.
10. Robertson, J. Electronic Structure and Core Exciton of Hexagonal Boron Nitride. *Phys. Rev. B* **1984**, *29*, 2131–2137.
11. Chen, Y.; Zou, J.; Campbell, S. J.; Le Caer, G. Boron Nitride Nanotubes: Pronounced Resistance to Oxidation. *Appl. Phys. Lett.* **2004**, *84*, 2430–2432.
12. Jhi, S.-H.; Kwon, Y.-K. Hydrogen Adsorption on Boron Nitride Nanotubes: A Path to Room-Temperature Hydrogen Storage. *Phys. Rev. B* **2004**, *69*, 245407.
13. Borek, T. T.; Ackerman, W.; Hua, D. W.; Paine, R. T.; Smith, D. M. Highly Microporous Boron Nitride for Gas Adsorption. *Langmuir* **1991**, *7*, 2844–2846.
14. Li, J.; Lin, J.; Xu, X.; Zhang, X.; Xue, Y.; Mi, J.; Mo, Z.; Fan, Y.; Hu, L.; Yang, X.; *et al.* Porous Boron Nitride with a High Surface Area: Hydrogen Storage and Water Treatment. *Nanotechnology* **2013**, *24*, 155603.
15. Ma, R.; Bando, Y.; Zhu, H.; Sato, T.; Xu, C.; Wu, D. Hydrogen Uptake in Boron Nitride Nanotubes at Room Temperature. *J. Am. Chem. Soc.* **2002**, *124*, 7672–7673.
16. Kim, J.; Han, J.; Seo, M.; Kang, S.; Kim, D.; Ihm, J. High-Surface Area Ceramic-Derived Boron-Nitride and Its Hydrogen Uptake Properties. *J. Mater. Chem. A* **2013**, *1*, 1014–1017.
17. Weng, Q.; Wang, X.; Zhi, C.; Bando, Y.; Golberg, D. Boron Nitride Porous Microbelts for Hydrogen Storage. *ACS Nano* **2013**, *7*, 1558–1565.
18. Janik, J. F.; Ackerman, W. C.; Paine, R. T.; Hua, D.-W.; Maskara, A.; Smith, D. M. Boron Nitride as a Selective Gas Adsorbent. *Langmuir* **1994**, *10*, 514–518.
19. Lei, W.; Portehault, D.; Liu, D.; Qin, S.; Chen, Y. Porous Boron Nitride Nanosheets for Effective Water Cleaning. *Nat. Commun.* **2013**, *4*, 1777.
20. Gorbachev, R. V.; Riaz, I.; Nair, R. R.; Jalil, R.; Britnell, L.; Belle, B. D.; Hill, E. W.; Novoselov, K. S.; Watanabe, K.; Taniguchi, T.; *et al.* Hunting for Monolayer Boron Nitride: Optical and Raman Signatures. *Small* **2011**, *7*, 465–468.
21. Yin, J.; Li, X.; Zhou, J.; Guo, W. Ultralight Three-Dimensional Boron Nitride Foam with Ultralow Permittivity and Superelasticity. *Nano Lett.* **2013**, *13*, 3232–3236.
22. Ikuno, T.; Sainsbury, T.; Okawa, D.; Fréchet, J. M. J.; Zettl, A. Amine-Functionalized Boron Nitride Nanotubes. *Solid State Commun.* **2007**, *142*, 643–646.
23. Lin, Y.; Williams, T. V.; Cao, W.; Elsayed-Ali, H. E.; Connell, J. W. Defect Functionalization of Hexagonal Boron Nitride Nanosheets. *J. Phys. Chem. C* **2010**, *114*, 17434–17439.
24. Zhi, C.; Bando, Y.; Terao, T.; Tang, C.; Kuwahara, H.; Golberg, D. Towards Thermoconductive, Electrically Insulating Polymeric Composites with Boron Nitride Nanotubes as Fillers. *Adv. Funct. Mater.* **2009**, *19*, 1857–1862.
25. Sainsbury, T.; Ikuno, T.; Okawa, D.; Pacilé, D.; Fréchet, J. M. J.; Zettl, A. Self-Assembly of Gold Nanoparticles at the Surface of Amine- and Thiol-Functionalized Boron Nitride Nanotubes. *J. Phys. Chem. C* **2007**, *111*, 12992–12999.
26. Jung, S. M.; Jung, H. Y.; Dresselhaus, M. S.; Jung, Y. J.; Kong, J. A Facile Route for 3D Aerogels from Nanostructured 1D and 2D Materials. *Sci. Rep.* **2012**, *2*, 849.
27. Schlienger, S.; Alauzun, J.; Michaux, F.; Vidal, L.; Parmentier, J.; Gervais, C.; Babonneau, F.; Bernard, S.; Miele, P.; Parra, J. B. Micro-, Mesoporous Boron Nitride-Based Materials Templated from Zeolites. *Chem. Mater.* **2012**, *24*, 88–96.
28. Dibandjo, P.; Bois, L.; Chassagneux, F.; Miele, P. Thermal Stability of Mesoporous Boron Nitride Templated with a Cationic Surfactant. *J. Eur. Ceram. Soc.* **2007**, *27*, 313–317.
29. Paine, R. T. Processing of Boron−Nitrogen Preceramic Polymers. *J. Inorg. Organomet. Polym.* **1992**, *2*, 183–195.
30. Lindquist, D. A.; Borek, T. T.; Kramer, S. J.; Narula, C. K.; Johnston, G.; Schaeffer, R.; Smith, D. M.; Paine, R. T. Formation and Pore Structure of Boron Nitride Aerogels. *J. Am. Ceram. Soc.* **1990**, *73*, 757–760.
31. Worsley, M. A.; Pauzauskie, P. J.; Olson, T. Y.; Biener, J.; Satcher, J. H., Jr.; Baumann, T. F. Synthesis of Graphene Aerogel with High Electrical Conductivity. *J. Am. Chem. Soc.* **2010**, *132*, 14067–14069.
32. Worsley, M. A.; Olson, T. Y.; Lee, J. R. I.; Willey, T. M.; Nielsen, M. H.; Roberts, S. K.; Pauzauskie, P. J.; Biener, J.; Satcher, J. H., Jr.; Baumann, T. F. High Surface Area, $sp^2$-Cross-Linked Three-Dimensional Graphene Monoliths. *J. Phys. Chem. Lett.* **2011**, *2*, 921–925.
33. Worsley, M. A.; Kucheyev, S. O.; Mason, H. E.; Merrill, M. D.; Mayer, B. P.; Lewicki, J.; Valdez, C. A.; Suss, M. E.; Stadermann, M.; Pauzauskie, P. J.; *et al.* Mechanically Robust 3D Graphene Macroassembly with High Surface Area. *Chem. Commun.* **2012**, *48*, 8428–8430.
34. Friederich, E.; Sittig, L. Herstellung Und Eigenschaften von Nitriden. *J. Inorg. Gen. Chem.* **1925**, *143*, 293–320.
35. Paine, R. T.; Narula, C. K. Synthetic Routes to Boron Nitride. *Chem. Rev.* **1990**, *90*, 73–91.
36. Hubáček, M.; Ueki, M. Chemical Reactions in Hexagonal Boron Nitride System. *J. Solid State Chem.* **1996**, *123*, 215–222.
37. Han, W.; Bando, Y.; Kurashima, K.; Sato, T. Synthesis of Boron Nitride Nanotubes from Carbon Nanotubes by a Substitution Reaction. *Appl. Phys. Lett.* **1998**, *73*, 3085–3087.
38. Han, W.-Q.; Brutchey, R.; Tilley, T. D.; Zettl, A. Activated Boron Nitride Derived from Activated Carbon. *Nano Lett.* **2004**, *4*, 173–176.
39. Aydoğdu, A.; Sevinç, N. Carbothermic Formation of Boron Nitride. *J. Eur. Ceram. Soc.* **2003**, *23*, 3153–3161.
40. Cullis, C. F.; Yates, J. Reaction of Carbon with Nitrogen. *Trans. Faraday Soc.* **1964**, *60*, 141–148.
41. Song, L.; Ci, L.; Lu, H.; Sorokin, P. B.; Jin, C.; Ni, J.; Kvashnin, A. G.; Kvashnin, D. G.; Lou, J.; Yakobson, B. I.; *et al.* Large Scale Growth and Characterization of Atomic Hexagonal Boron Nitride Layers. *Nano Lett.* **2010**, *10*, 3209–3215.
42. Li, C.; Bando, Y.; Zhi, C.; Huang, Y.; Golberg, D. Thickness-Dependent Bending Modulus of Hexagonal Boron Nitride Nanosheets. *Nanotechnology* **2009**, *20*, 385707.
43. Kim, K.; Lee, Z.; Malone, B. D.; Chan, K. T.; Alemán, B.; Regan, W.; Gannett, W.; Crommie, M. F.; Cohen, M. L.; Zettl, A. Multiply Folded Graphene. *Phys. Rev. B* **2011**, *83*, 245433.
44. Ortolani, L.; Cadelano, E.; Veronese, G. P.; Boschi, C. D. E.; Snoeck, E.; Colombo, L.; Morandi, V. Folded Graphene Membranes: Mapping Curvature at the Nanoscale. *Nano Lett.* **2012**, *12*, 5207–5212.
45. Arenal, R.; Kociak, M.; Zaluzec, N. J. High-Angular-Resolution Electron Energy Loss Spectroscopy of Hexagonal Boron Nitride. *Appl. Phys. Lett.* **2007**, *90*, 204105.
46. Ahn, C. C.; Krivanek, O. L. *EELS Atlas: A Reference Guide of Electron Energy Loss Spectra Covering All Stable Elements*; Gatan: Warrendale, PA, 1983.
47. Nemanich, R. J.; Solin, S. A.; Martin, R. M. Light Scattering Study of Boron Nitride Microcrystals. *Phys. Rev. B* **1981**, *23*, 6348–6356.
48. Brunauer, S.; Emmett, P. H.; Teller, E. Adsorption of Gases in Multimolecular Layers. *J. Am. Chem. Soc.* **1938**, *60*, 309–319.

49. Bartnitskaya, T. S.; Kosolapova, T. Ya.; Kurdyumov, A. V; Oleinik, G. S.; Pilyankevich, A. N. Structure and Some Properties of Fine-Grained Graphite-like Boron Nitride. *J. Less-Common Met.* **1986**, *117*, 253–258.
50. Yoon, S. J.; Jha, A. Vapour-Phase Reduction and the Synthesis of Boron-Based Ceramic Phases. Part II: The Synthesis of Hexagonal Boron Nitride Phase. *J. Mater. Sci.* **1996**, *31*, 2265–2277.
51. Han, W.-Q.; Yu, H.-G.; Liu, Z. Convert Graphene Sheets to Boron Nitride and Boron Nitride–Carbon Sheets *via* a Carbon-Substitution Reaction. *Appl. Phys. Lett.* **2011**, *98*, 203112.
52. Golberg, D.; Bando, Y.; Kurashima, K.; Sato, T. $MoO_3$-Promoted Synthesis of Multi-Walled BN Nanotubes from C Nanotube Templates. *Chem. Phys. Lett.* **2000**, *323*, 185–191.
53. Han, W.-Q.; Mickelson, W.; Cumings, J.; Zettl, A. Transformation of $B_xC_yN_z$ Nanotubes to Pure BN Nanotubes. *Appl. Phys. Lett.* **2002**, *81*, 1110–1112.
54. Dean, C. R.; Young, A. F.; Meric, I.; Lee, C.; Wang, L.; Sorgenfrei, S.; Watanabe, K.; Taniguchi, T.; Kim, P.; Shepard, K. L.; *et al.* Boron Nitride Substrates for High-Quality Graphene Electronics. *Nat. Nanotechnol.* **2010**, *5*, 722–726.
55. Geim, A. K.; Grigorieva, I. V. van der Waals Heterostructures. *Nature* **2013**, *499*, 419–425.
56. Ci, L.; Song, L.; Jin, C.; Jariwala, D.; Wu, D.; Li, Y.; Srivastava, A.; Wang, Z. F.; Storr, K.; Balicas, L.; *et al.* Atomic Layers of Hybridized Boron Nitride and Graphene Domains. *Nat. Mater.* **2010**, *9*, 430–435.